ACS OMEGA

http://pubs.acs.org/journal/acsodf

Article

Investigation of Antimicrobial Activity and Biocompatibility of Biogenic Silver Nanoparticles Synthesized using *Syzigyum cymosum* Extract

Kazi Mustafa Mahmud, Md. Monir Hossain, Shakil Ahmed Polash, Masato Takikawa, Md Salman Shakil, Md Forhad Uddin, Morshed Alam, Mohammad Mahfuz Ali Khan Shawan, Tanushree Saha, Shinji Takeoka, Md. Ashraful Hasan,* and Satya Ranjan Sarker*

Cite This: *ACS Omega* 2022, 7, 27216–27229

Read Online

ACCESS | Metrics & More | Article Recommendations | Supporting Information

ABSTRACT: Nanotherapeutics has emerged as the most sought after approach to tackle the menace of drug-resistant pathogenic bacteria. Among others, biogenic silver nanoparticles (bAgNPs) synthesized using medicinal plant extracts demonstrate promising antibacterial propensity with excellent biocompatibility. Herein, bAgNPs were synthesized through the green chemistry approach using *Syzygium cymosum* leaf extract as a reducing agent at different pH values (i.e., 5, 7, 8, and 10). The average size of bAgNPs synthesized at pH 5, 7, 8, and 10 was 23.3, 21.3, 17.2, and 35.3 nm, respectively, and all the nanoparticles were negatively charged. Their antibacterial potential was investigated against *Bacillus subtilis*, *Escherichia coli* DH5α, *E. coli* K12, enteropathogenic *E. coli*, and *Salmonella typhi*. The highest antibacterial activity was exhibited by bAgNPs synthesized at pH 8 against all the tested bacterial strains, which can be attributed to their small size and greater surface area to volume ratio. The bAgNPs demonstrated the highest zone of inhibition (29.5 ± 0.8 mm) against *B. subtilis* through oxidation of membrane fatty acids that resulted in the formation of the malondialdehyde−thiobarbituric acid (MDA−TBA) adduct. However, bAgNPs demonstrated excellent hemocompatibility with rat and human red blood cells. Biogenic AgNPs synthesized at pH 8 also exhibited biocompatibility in terms of liver and kidney function biomarkers. Furthermore, hematoxylin and eosin staining of the tissue sections of vital organs (i.e., liver, kidneys, lungs, heart, spleen, and brain) also confirmed the biocompatibility of bAgNPs.

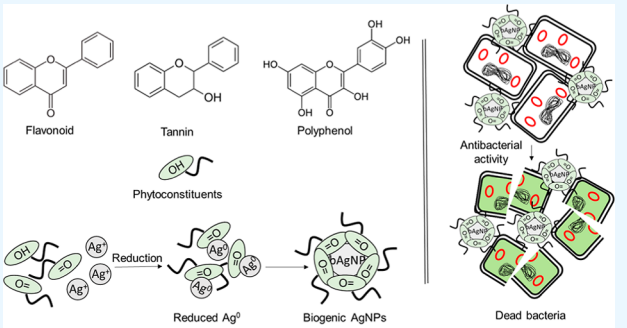

Formation of bAgNPs and mechanism of their antibacterial propensity

1. INTRODUCTION

Pathogenic bacteria, which are gaining resistance to chemically synthesized antibiotics, are the real threat to the existence of mankind. On the other hand, many chemically synthesized therapeutic agents are responsible for the systemic toxicity.[1] Among them, antibiotics are the most commonly prescribed drugs to treat severe and potentially fatal infections. The abuse of antibiotics is mainly responsible for the increasing bacterial resistance and other side effects.[2] For example, antibiotics sometimes interact with other drugs and make those drugs or antibiotics less effective, which results in adverse effects including nausea, diarrhea, and stomach pain leading to dehydration and other problems.[2] Furthermore, antibiotics are also associated with hepatotoxicity (e.g., DILI, cholestatic injury, cirrhosis, and hepatitis)[3] and nephrotoxicity (acute kidney injury).[1] Hence, it is urgently needed to find biocompatible antibacterial agents that will be effective against a wide spectrum of bacteria.

The advancement in nanoscience and technology is contributing immensely to design, synthesis, and fabrication of new nanomaterials. Nanomaterials can also be modified at the atomic and molecular level to generate nanostructures with enhanced functionality.[4] Nanoparticles have tremendous advantages due to their tiny size and large surface-to-volume ratio. This helps to attain differences in both physical and chemical properties from the bulk of the same compound.[5] Thus, by controlling shape and size at the nanometer scale, materials with a unique application can be obtained. Among other nanoparticles, silver nanoparticles (AgNPs) are well known for their antimicrobial potential in wound dressing, catheters, cardiovascular implants, and dental composites.[6] Several methods (i.e., physical, chemical, and biological) have been used to synthesize AgNPs. However, the physical and

Received: March 29, 2022
Accepted: July 5, 2022
Published: July 25, 2022

Scheme 1. Outline of the Synthesis of bAgNPs Using *S. cymosum* Leaf Extract

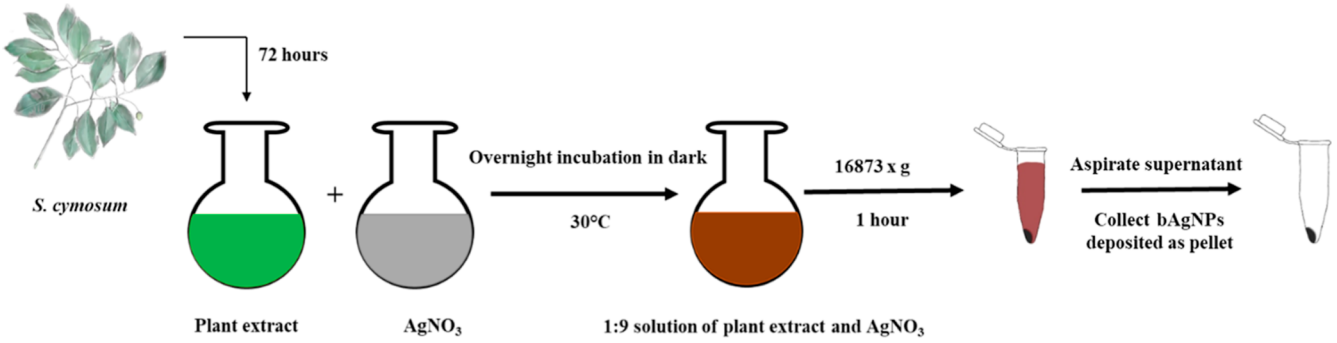

chemical methods are relatively expensive and tedious, require high pressure and temperature, and use environmentally and biologically toxic and hazardous chemicals and solvents.[7] In fact, plants stand out to be the most preferred way to synthesize nanoparticles. It has been proven to be better than chemical and physical methods since it is environment friendly, reduces the production of toxic waste materials, excludes the application of high pressure, energy, or temperature, and also can simply be scaled up for large-scale production.[8] In addition, phytoconstituents reduce metal ions at a faster rate and form more stable metal nanoparticles than microorganisms.[9] The green synthesis approach also provides better control over crystal growth and their stabilization.[10] Several parameters such as $AgNO_3$ concentration, medium pH, duration of reaction, and light irradiation influence the morphology and size of the synthesized AgNPs.[11] pH modulates the surface charge of the bioactive molecules and capping agents, which control the average size and morphology of biologically synthesized AgNPs. Moreover, pH of the reaction medium also influences the capability of phytoconstituents to incorporate and reduce metal ions.[12]

Biogenic silver nanoparticles (bAgNPs) are one of the most promising antibacterial agents. Hence, it is necessary to thoroughly investigate the biocompatibility of bAgNPs for their clinical trials and commercial applications. The cytotoxicity of bAgNPs can be minimum due to the presence of biocompatible phytoconstituents as capping agents.[9] Thus, the inherent biocompatibility of conjugated phytoconstituents makes the bAgNPs appropriate for different clinical applications.[13] In the previous study, bAgNPs showed excellent hemocompatibility against human and rat red blood cells (RBCs). Rats treated with bAgNPs demonstrated no significant toxicity in terms of hematological and biochemical parameters.[14,15]

Syzygium cymosum is a clove-like plant that is widely distributed in tropical and subtropical areas. *S. cymosum* and other members of the genus Syzygium have antibacterial, antifungal, antimalarial, antidiarrheal, and antioxidant propensity.[16−20] Phytoconstituents including alkaloids, carbohydrates, glycosides, flavonoids, and tannins are present in S. cymosum.[21] Thus, the secondary metabolites could contribute as reducing as well as capping agents to prepare AgNPs from $AgNO_3$ solution. Previously, AgNPs were synthesized using different plant extracts (e.g., lemongrass, geranium, *alfa alfa*, and so on), and their antimicrobial potential was also investigated.[22] In this study, we synthesized bAgNPs using *S. cymosum* extract as the source of reducing agent under a pH-controlled environment. The extract of *S. cymosum* has never been used for the synthesis of AgNPs. We synthesized bAgNPs using *S. cymosum* leaf extract at pH 5, 7, 8, and 10. The as-synthesized bAgNPs were characterized by UV−visible and Fourier transform infrared (FTIR) spectroscopy, powder X-ray diffraction, zetasizer analysis, and scanning transmission electron microscopy. The antibacterial potential of bAgNPs against both Gram-positive and Gram-negative bacteria was investigated through broth dilution, disk diffusion, CellTox green, and trypan blue dye exclusion assay. The mechanism of antibacterial activity of bAgNPs was determined through lipid peroxidation (LPO) assay. RBCs of both male Wister rats and humans were used to investigate the hemocompatibility of the as-synthesized bAgNPs. The biocompatibility of bAgNPs was investigated in vivo using male Wister rats.

2. MATERIALS AND METHODS

2.1. Materials. Silver nitrate ($AgNO_3$) was purchased from Sigma-Aldrich (USA). Hydrochloric acid (HCl) and sodium hydroxide (NaOH) were obtained from Merck (India). Agar powder was bought from Titan Biotech Limited (India). Sodium chloride (NaCl), peptone, and yeast extract were obtained from Unichem (China). CellTox green dye was obtained from Alfa Aesar (UK). Thiobarbituric acid (TBA) and trichloroacetic acid (TCA) were purchased from Merck (Germany) and J.T. Baker (USA), respectively. Gram-positive bacterial strain (i.e., *Bacillus subtilis*) and Gram-negative bacterial strains (i.e.,*Escherichia coli* DH5α, enteropathogenic *E. coli* (EPEC), *E.coli* K12, and *S. typhi*) were obtained from the Department of Biotechnology and Genetic Engineering, Jahangirnagar University, Dhaka, Bangladesh. Male Wister albino rats (weighing between 199 and 260 g) were collected from the Department of Biochemistry and Molecular Biology, Jahangirnagar University, Dhaka, Bangladesh. Reagents required for the biochemical analysis of serum ALT, AST, ALP, albumin, uric acid, creatinine, cholesterol, and triglycerides (TGs) were purchased from Liner (Spain). A HDL cholesterol analysis kit was bought from Randox (U.K.) and a serum γ-GT analysis kit was purchased from Vitro Scient (Egypt).

2.2. Synthesis of bAgNPs. *S. cymosum* leaf extract was used to synthesize bAgNPs (Scheme 1). Fresh leaves of *S. cymosum* were washed assiduously with distilled water, dried in the sun, and ground into fine powder. For the preparation of 10% aqueous leaf extract, 20 g of leaf powder was mixed with 200 mL of distilled water and incubated for 72 h upon constant stirring. The extract was filtered using Whatman no.1 filter paper and stored at 4 °C temperature. The as-prepared aqueous leaf extract was then mixed with freshly prepared 10 mM $AgNO_3$ solution at a ratio of 1:9, and the pH of the

https://doi.org/10.1021/acsomega.2c01922
ACS Omega 2022, 7, 27216−27229

mixture was adjusted to 5, 7, 8, and 10. All the mixtures were incubated for 24 h at 30 °C under constant stirring in a dark chamber to prevent the photoactivation of $AgNO_3$. Here, the plant extract acted as a reducing agent to reduce Ag^+ to Ag^0, which was confirmed by the conversion of the colorless solution to brown color.[23] The reaction mixtures were centrifuged at 16,873 *g* for 1 h at room temperature to eliminate the unconjugated $AgNO_3$ and plant extract. The as-synthesized bAgNPs were precipitated as pellets. The supernatant was aspirated to collect the precipitated bAgNPs. Finally, bAgNPs were washed twice with MQ water and redispersed.

2.3. Characterization of bAgNPs. A UV−visible spectrophotometer (Specord205, Analytik Jena, Germany) and an FTIR spectrometer (IRPrestige-21, SHIMADZU, Japan) were used to characterize the as-synthesized bAgNPs. The nanoparticles were sonicated for 30 min in a bath-type sonicator prior to measuring their ζ potential and hydrodynamic size using a ζ size analyzer (Nano-ZS90; Spectris PLC, Egham, England). A transmission electron microscope having a field emission gun (HF-2200; Hitachi, Tokyo, Japan) together with an energy-dispersive X-ray spectrometer (EDAX Genesis; AMETEK, Pennsylvania, USA) operating at 200 kv was used to determine the shape, morphology, and composition of bAgNPs. A scanning transmission electron microscopy (TEM) unit was also equipped with a high-angle annular dark field (HAADF) detector and secondary electron (SE) detector. All the bAgNPs were observed under electron microscopy without staining with any staining agent or coating with any conductive metal. The powder X-ray diffraction (XRD) patterns of bAgNPs were achieved by a powder X-ray diffractometer (GNR X-ray Explorer, Italy) according to our previously published protocol.[14,15]

2.4. Antimicrobial Activity Assay. The bacterial strains used to investigate the antibacterial potential of the as-synthesized bAgNPs synthesized at different pH values include Gram-positive bacteria (i.e., *B. subtilis*) and Gram-negative acteria (i.e., *E. coli* DH5α, enteropathogenic *E. coli* (EPEC), *E.coli* K12, and *Salmonella typhi* AF4500). The antibacterial activity of bAgNPs was evaluated in terms of their zone of inhibition (ZOI) in millimeter (mm), minimum inhibitory concentration (MIC) values, trypan blue dye exclusion assay, and CellTox green cytotoxicity assay.

2.4.1. Determination of the Minimum Inhibitory Concentration Value. The lowest amount of bAgNPs required to stop the growth of a bacterial strain is considered as the MIC value. The MIC value of bAgNPs synthesized at different pH values was evaluated according to our previously published protocol.[14,24] Briefly, the bacterial strains were grown overnight and 10 μL from each of the bacterial cultures was mixed with 990 μL of freshly prepared Luria Bertani (LB) broth and incubated at 37 °C and 120 rpm for 4 h. Then, different amounts of bAgNPs (i.e., 0.125, 0.25, 0.5, 1, 2, 3, 3.5, 5, and 6 μg) synthesized at different pH values (i.e., 5, 7, 8, and 10) were added to the bacterial culture and incubated overnight at 37 °C and 120 rpm. The optical density (OD) of respective bacterial strains was determined using a UV−vis spectrophotometer (Optizan, POP, Korea) at 600 nm to measure the MIC values of the as-synthesized bAgNPs.

2.4.2. Determination of the ZOI. The antibacterial activity of the as-synthesized bAgNPs against both Gram-positive and Gram-negative bacteria was evaluated by the disk diffusion method according to our previously published protocol.[25] Briefly, LB broth was used to cultivate all the tested bacterial strains at 37 °C and 120 rpm overnight. The respective bacterial culture (100 μL) was uniformly spread on LB agar plates. Different amounts of bAgNPs (i.e., 60, 40, and 20 μg) were drop-cast on metrical filter paper disks before placing on LB agar plates containing uniformly spread bacteria. The LB agar plates were then incubated at 37 °C temperature overnight. The antibacterial propensity of bAgNPs was determined by measuring the clear zones around the disks. The diameter of the clear zones was measured with slide calipers at different time intervals such as 12 and 24 h.

2.4.3. Trypan Blue Dye Exclusion Assay. Trypan blue dye exclusion assay was performed to determine the cell viability. The trypan blue dye exclusion assay was performed according to our previously established protocol with some modifications.[26] Briefly, two pathogenic and three nonpathogenic bacterial strains were incubated overnight in LB media (1×10^6 CFU/mL). The bacterial cultures (80 μL of each strain) were mixed separately with 20 μL of bAgNPs synthesized at pH 8 and incubated at 37 °C and 120 rpm for 1.5 h. Trypan blue solution (0.4%) was then mixed with bAgNP-treated bacterial cultures at a ratio of 1:1 and incubated for 15 min at room temperature before imaging live and dead bacterial cells under a phase-contrast microscope (Olympus BX50 fluorescence microscope, Olympus, Japan) under 40× magnification.

2.4.4. CellTox Green Assay. Fluorescence dye (i.e., CellTox green) penetrates through the damaged bacterial cell membrane and emits green fluorescence upon binding with deoxyribonucleic acid (DNA).[27] CellTox green assay was performed according to our established protocol.[14] In brief, bacterial culture was incubated overnight and diluted with LB broth to set the concentration to 1×10^7 CFU/mL. Then, 20 μL of bAgNPs synthesized at different pH values (i.e., 5, 7, 8, and 10) was mixed with 80 μL (1×10^7 CFU/mL) of the respective bacterial strains, and the final volume up was made to 1 mL with LB broth before incubating at 37° C and 120 rpm for 2 hours. The CellTox green reagent (1 μL, 2×) was mixed with bAgNP-treated bacterial culture and placed in the dark for another 30 minutes at room temperature. An aliquot of CellTox-treated bacterial culture (i.e., 20 μL) was used to detect the dead bacteria under a fluorescence microscope (Olympus BX50 fluorescence microscope, Olympus, Japan). The remaining bacterial culture was used to quantify the fluorescence intensity of green fluorescent dye using a spectrofluorophotometer (SHIMADZU RF-6000, Japan) at 490 nm. The control experiments were also carried out (bAgNPs, bacteria, and LB media) without CellTox green along with the treatment groups. All experiments were performed in triplicate.

2.5. Lipid Peroxidation Assay. The lipid peroxidation (LPO) propensity of bAgNPs synthesized at pH 8 was performed according to the established protocol.[26] Briefly, 1 mL of each of the tested bacterial strains was mixed with 200 μL of bAgNPs and incubated at room temperature for 2 h. The bacterial cultures were then treated with 2 mL of 10% trichloroacetic acid (TCA) and centrifuged at 10,416 *g* for 35 min at room temperature to separate the insoluble components of cells. The supernatant containing malondialdehyde was taken in a new tube and mixed with 4 mL of 0.67% freshly prepared thiobarbituric acid (TBA) solution and incubated in steaming water bath for 10 min to facilitate the formation of the malondialdehyde−TBA adduct before cooling down to

https://doi.org/10.1021/acsomega.2c01922
ACS Omega 2022, 7, 27216−27229

room temperature. The absorbance of the malondialdehyde−TBA adduct was measured at 532 nm using a UV−vis spectrophotometer (Specord 205, Analytik Jena, Germany).

2.6. Hemocompatibility Assay. The hemocompatibility of bAgNPs synthesized at four different pH (i.e., 5, 7, 8, and 10) was investigated against human and rat RBCs according to the previously established protocol with some modification.[26] Briefly, 6 mL of human blood was collected through the venipuncture method and preserved in a tube containing 10% EDTA as an anticoagulant. On the other hand, two rats were anesthetized with 0.3 mL/250 g ketamine/xylazine (100 mg/mL ketamine + 20 mg/mL xylazine), and ∼6 mL of blood (3 mL from each rat) was drawn from the inferior vena cava and collected in a tube containing 10% EDTA. Both the blood samples were then centrifuged at 500 g for 10 min at room temperature to separate RBCs from serum. The serum was aspirated followed by the resuspension of precipitated RBCs in 5 mL-phosphate-buffered saline (PBS) and centrifuged at 500 g for 10 min. The RBCs were washed twice with 150 mM NaCl solution at 3000 g for 3 min. RBC suspension (0.1 mL) was then mixed with 60 μg of bAgNPs synthesized at different pH values (i.e., 5, 7, 8, and 10) and incubated for 30 min at 37 °C under gentle shaking. The mixture of RBCs and bAgNPs was then centrifuged at 4000 rpm for 5 min. The supernatant was collected, and the absorbance was measured at 570 nm. In this experiment, RBCs incubated with PBS and distilled water were considered as negative and positive controls, respectively. The whole experiment was repeated three times, and the degree of lysis was evaluated. The percentage hemolysis was determined by using the following formula

$$\%\ \text{hemolysis} = \frac{A_{\text{sample}} - A_{\text{negative control}}}{A_{\text{positive control}} - A_{\text{negative control}}} \times 100$$

where A_{sample}, $A_{\text{positive control}}$, and $A_{\text{negative control}}$ are the absorbances of the sample, positive control, and negative control, respectively.

2.7. In vivo Biocompatibility Assay. Albino Wister male rats (16−24 weeks old) weighing between 199 and 260 g were used in the study. Forty (40) rats were divided into 10 groups (i.e., groups A−J and $n = 4$). The rats were bred and reared in the animal house facility of the Department of Biochemistry and Molecular Biology, Jahangirnagar University, at controlled room temperature (23 ± 2 °C) and humidity (55 ± 7%) with a natural 12 h day−night cycle.[28] The experiments were conducted according to the ethical guidelines approved by the Bangladesh Association for Laboratory Animal Science. All the rats were maintained under the institutional guidelines for the care and use of animals for scientific purposes and following the recommendations from Helsinki Declaration. The experiments in this study were approved by the Biosafety, Biosecurity, and Ethical Committee of Jahangirnagar University, Savar, Dhaka, Bangladesh (Ethical clearance number: BBEC, JU/M 2019 (9)1).

The bAgNPs synthesized at pH 8 were administered through the intravenous route via the tail vein. The control group (i.e., group J) received 1 mL of distilled water, while the treatment groups (i.e., group A−I) were treated with different concentrations of bAgNPs. Among all the bAgNPs synthesized at different pH values, the nanoparticles synthesized at pH 8 were selected for the in vivo cytotoxicity study since they showed the highest antimicrobial activity against all the bacterial strains. Experimental rats were sacrificed at three different time points (i.e., 1, 7, and 28 days) to evaluate the acute, sub-acute, and chronic cytotoxic effects. During the test period, the experimental rats were observed for any abnormal signs and death. At the end of the respective experimental period, the rats were deeply anesthetized with ketamine hydrochloride injection (100 mg/kg body weight) followed by dissection. Blood samples (∼4.2 mL) were collected using a heparinized syringe (size: 6 mL) from inferior vena cava. The liver, kidney, heart, brain, lungs, and spleen of the experimental rats were then dissected out immediately and preserved in 10% formalin for histopathology studies. For biochemical analysis, the blood samples were transferred into dry test tubes and allowed to coagulate at room temperature for 30 min before centrifuging at 538 g for 10 min to separate the serum. The serum was stored at −20 °C for further biochemical analysis.

2.7.1. Biochemical Analysis. Different biomarkers for liver (i.e., serum ALT, ALP, AST, γ-GT, and albumin) and kidney (i.e., serum creatinine and uric acid), and lipid profile (i.e., TC, TG, LDL-C, and HDL-C) were measured in according to the manual provided with the reagent kits.

2.7.2. Histopathological Analysis. Histopathological analysis was performed to evaluate the toxicity of the bAgNPs by resecting the brain, liver, kidney, heart, spleen, and lung tissue of the experimental rats. All specimens were preserved in 10% buffered formalin (10% neutral buffered formalin). Tissues collected from the aforementioned organs were then sliced (about 5 μm thick), fixed, dehydrated, paraffin-embedded, and stained with hematoxylin and eosin (H&E) stain and observed under a standard light microscope (Olympus BX50 Fluorescence Microscope, Olympus, Japan) under 40× magnification.

2.8. Statistical Analysis. All data were statistically analyzed using GraphPad Prism 5.0 (GraphPad Software Inc., San Diego, CA), OriginPro 8.5, and Microsoft Excel 2016. The values were presented as means ± SEM from at least three independent experiments. Dunnet test was performed for posthoc comparison, and $p < 0.05$ was considered statistically significant.

3. RESULTS AND DISCUSSION

3.1. Characterizations of bAgNPs. The formation of bAgNPs were confirmed primarily by the change in color of $AgNO_3$ solution. When $AgNO_3$ solution was incubated with *S. cymosum* leaf extract for 24 h, the colorless solution gradually turned yellow to dark brown as shown in Figure S1a. The dark brown color appeared due to the surface plasmon resonance, a common property of AgNPs.[23] *S. cymosum* contains tannin, alkaloids, carbohydrates, flavonoids, glycosides, saponins, and steroids.[21] The presence of these secondary metabolites contributes to the reduction of Ag^+ to Ag^0. Previous studies reported that leaves containing tannin, glycosides, proteins, alkaloids, flavones reduce silver ions to silver atoms (i.e., Ag^+ to Ag^0) and subsequently form nanoparticles.[29] It is assumed that bioactive molecules or reducing agents (e.g., flavonoids, alkaloids, tannins, phenols, glycosides, etc.) of *S. cymosum* leaf extract are reconverted from NADPH to $NADP^+$, which donates electrons to reduce Ag^+ to Ag^0. The obtained Ag^0 then nucleates into small clusters, which form particles as bAgNPs.[30]

The electrons of a metal (i.e., silver) surface oscillate when nanoparticles are exposed to light of a specific wavelength and are responsible for the strong scattering and absorption properties of bAgNPs.[31] Thus, the synthesis of bAgNPs was

https://doi.org/10.1021/acsomega.2c01922
ACS Omega 2022, 7, 27216−27229

confirmed by analysis of UV−visible spectra, and the λ_{max} value was determined. As demonstrated in Figure S1a,a high-intensity surface plasmon resonance (SPR) band was observed at ∼435, ∼410, ∼412, and ∼405 nm for bAgNPs synthesized at pH 5, 7, 8, and 10, respectively, that are within the characteristic wavelength range of the synthesized bAgNPs.[32]

Moreover, the SPR band intensity increased with the increasing pH values (i.e., 5−10) (Figure S1a). The spectral position of the SPR band was affected by pH of the reaction solution. An increase in the solution pH from 5 to 10 brought about a blueshift of the SPR band that shifted from ∼435 to ∼405 nm (Figure S1a). These spectral changes can be ascribed to a decrease in the size of metal nanoparticles, and alkaline conditions generate small-size bAgNPs[33] (Figure S1). The absorption spectrum of bAgNPs synthesized at pH 5 exhibited a significant redshift of the SPR band [i.e., shifted to higher wavelengths (435 nm)], indicating a low intensity and distinct morphology (i.e., size and shape) of the synthesized nanoparticles.[34] Assuming that a shift in the SPR peak indicates a change in the size of AgNPs, any shift of the SPR peak toward the shorter wavelength is accompanied by a decrease in the size of the as-prepared bAgNPs. Hence, we conclude that the increasing pH of the solution results in the formation of nanoparticles with smaller size and vice versa (Figure S1a and Table S7). On the other hand, broadening of the surface plasmon resonance peak indicates the existence of a wide range of particle sizes in the solution.[35] Again, in a high-pH environment, the rate of reduction is high. Conversely, in a low-pH (below 5) environment, oxidation prevails over the reduction process. In a very high-pH (i.e., ≥9, 10) environment, the rate of reduction is very fast, resulting in the aggregation of the nanoparticles.[36] Hence, at pH 10, the size of bAgNPs was large due to the severe aggregation of the particles (Figure S1b and Table S7). Hence, pH 8 solution is highly desirable in order to synthesize small-size nanoparticles. Additionally, our as-prepared bAgNPs demonstrated similar SPR (surface plasmon resonance) bands (ranging from 400 to 450 nm) with those of other AgNPs reported in the literature.[37,38] However, the particle size was different, which can be attributed to the presence of different plant secondary metabolites in *S. cymosum* extract.[39] The average size of bAgNPs synthesized at pH 8 was smaller than most of the bAgNPs reported in the literature.[40,41]

The morphology of the bAgNPs synthesized at different pH values (i.e., 5, 7, 8, and 10) was further analyzed by scanning TEM. The scanning TEM images of the synthesized bAgNPs at the 50 nm scale are shown in Figure S1b. Respective TEM images showed that most of the bAgNPs were spherical-shaped and the average size of bAgNPs synthesized at pH 5, 7, 8, and 10 was 23.3, 21.3, 17.2, 35.3 nm, respectively, as obtained from the particle size distribution (PSD) histogram.

FTIR spectroscopy was used to characterize the functional groups of *S. cymosum* phytoconstituents (e.g., flavonoids, alkaloids, and so on) responsible for the reduction of $AgNO_3$ to generate bAgNPs. The FTIR spectra (Figure S2) showed several major peaks at 2770, 2404, 1766, and 1388 cm^{-1} for $AgNO_3$; 3739, 2914, 2350, 1529, and 1381 cm^{-1} for the as-synthesized bAgNPs; and 3742, 2925, 2350, 1525, and 1348 cm^{-1} for leaf extract. The comparison of FTIR spectra of bAgNPs with those of plant extract and $AgNO_3$ showed that there was minute shifting of all the bands. The shift of the bands could be due to the formation of nanoparticles. Moreover, a peak appeared at around 1381 cm^{-1} in the spectra of bAgNPs synthesized at different pH values, which resembled the peak at 1388 cm^{-1} of $AgNO_3$ and corresponds to N−O stretch.[42] The intense peak at 2350 cm^{-1} for both bAgNPs and plant extract indicates the presence of flavonoids and compounds with an unsaturated C═C structure in the aromatic ring structure.[32] The peak at 2914 cm^{-1} is associated with C−H stretching of carbohydrates.[43] Furthermore, plant extract and bAgNPs also showed a similar peak at 3742 cm^{-1}, indicating the presence of the free silanol (similar to the alcohol group) group.[44] The resemblance in the FTIR spectra of bAgNPs with those of plant extract confirms the synthesis of bAgNPs from *S. cymosum* leaf extract.

Grain size, crystallinity, and orientation of the as-synthesized bAgNPs were obtained from XRD spectra (Figure S3) that conspicuously demonstrate the characteristic diffraction peaks related to crystalline silver. The diffraction peaks at around 27, 34, 38, and 46° correspond to the Miller indices (111), (200), (220), and (311), respectively, of the as-synthesized bAgNPs and confirm face-centered cubic (FCC) crystalline elemental silver. The attained results match with the Joint Commission of Powder Diffraction Standards (JCPDS) database bearing file no. 04−0783.[45] The crystalline grain size of the as-synthesized bAgNPs was estimated from the Debye−Scherrer equation $D = (K\lambda/\beta \cos \theta)$ [where D is the mean crystalline size of the particle, K is the shape factor whose value is 0.9, λ is the wavelength of the X-ray radiation source (i.e., 0.154 nm), β is $(\pi/180)$* FWHM, and θ is the Bragg angle]. The average particle sizes determined using Scherer's equation were 29, 27.7, 23.5, and 32.71 nm for bAgNPs synthesized at pH 5, 7, 8, and 10, respectively. The sharp peaks in XRD spectra can be ascribed to the biomolecules of plant extracts. However, the remaining star-marked peaks might indicate the presence of organic impurities in the sample.[32] The XRD data also suggest that the crystal size of bAgNPs decreased with the increasing pH values (i.e., 5 to 8) except at pH 10, which is attributed to the aggregation of bAgNPs at pH > 8. Hence, small and monodispersed nanoparticles were formed at pH 8.

The average hydrodynamic diameter of bAgNPs synthesized at pH 5, 7, 8, and 10 was 121 ± 64, 94 ± 58, 243 ± 98, and 93 ± 59 nm, respectively (Table S1). The size of the bAgNPs observed using scanning TEM was smaller than that of the hydrodynamic diameter obtained from dynamic light scattering (DLS) measurement. This is because TEM provides information about the inorganic core only. On the other hand, the hydrodynamic diameter of nanoparticles is influenced by the interaction between electric dipole of solvent and conjugated bioactive molecules of the phytoconstituents.[32] The polydispersity index (PDI) values of the bAgNPs synthesized at pH 5, 7, 8, and 10 were 0.296, 0.620, 0.449, 0.629, respectively (Table S1). Particles with a PDI value less than 0.50 are generally considered as "good"-quality particles.[46] The ζ potentials of bAgNPs synthesized at pH 5, 7, 8, and 10 were −32 ± 1, −23 ± 2, −32 ± 3, and −27 ± 1 mv, respectively (Table S1).The negative ζ potential of bAgNPs can be due to the adsorption of bioactive molecules on the surface of particles.[47] The pH of the solution is directly related to the stability of the nanoparticles. Any change in pH can alter the double-layer properties that directly influence the ζ potential of the system, increasing the chances of flocculation or coagulation because nanoparticles are stable near the isoelectric point.[48] Additionally, the ζ potential near −30 mV is good for physical stability[48] of nanoparticles (Figure S1a and Table S1), and the stability of bAgNPs did not significantly

https://doi.org/10.1021/acsomega.2c01922
ACS Omega 2022, 7, 27216−27229

Table 1. Antibacterial Activity (i.e., MIC Values and the ZOI) of bAgNPs

	MIC (μg)				ZOI (mm)					
name of strain	bAgNPs at pH 5	bAgNPs at pH 7	bAgNPs at pH 8	bAgNPs at pH 10	bAgNPs at pH 5 (60 μg)	bAgNPs at pH 7 (60 μg)	bAgNPs at pH 8 (60 μg)	bAgNPs at pH 10 (60 μg)	plant extract (60 μg)	$AgNO_3$
B. subtilis	0.125	0.125	0.125	0.125	16.87± 0.17	25.87 ± 0.7	29.5 ± 0.7	29 ± 1.41	6.5 ± 0	12 ± 0.25
E. coli DH5α	0.125	0.125	0.125	0.125	15.66 ± 0.94	15.85± 0.23	20.83 ± 0.23	16.87 ± 0.25	7 ± 0	13.67 ± 0.5
E. coli K12	0.125	0.125	0.125	0.125	11 ± 1.41	10.33 ± 1.17	12.48 ± 0.58	8.5 ± 0.82	6 ± 0	11.17 ± 0.37
EPEC	0.125	0.125	0.125	0.125	13.99 ± 0.23	14.5 ± 0.71	17.83 ± 1.64	13.41 ± 0.12	6.5 ± 0	12.25 ± 0.17
S. typhi	0.125	0.125	0.125	0.125	10.25 ± 0.41	8.81 ± 0.44	14 ± 1.82	9.5 ± 0.71	6 ± 0	12 ± 0.67

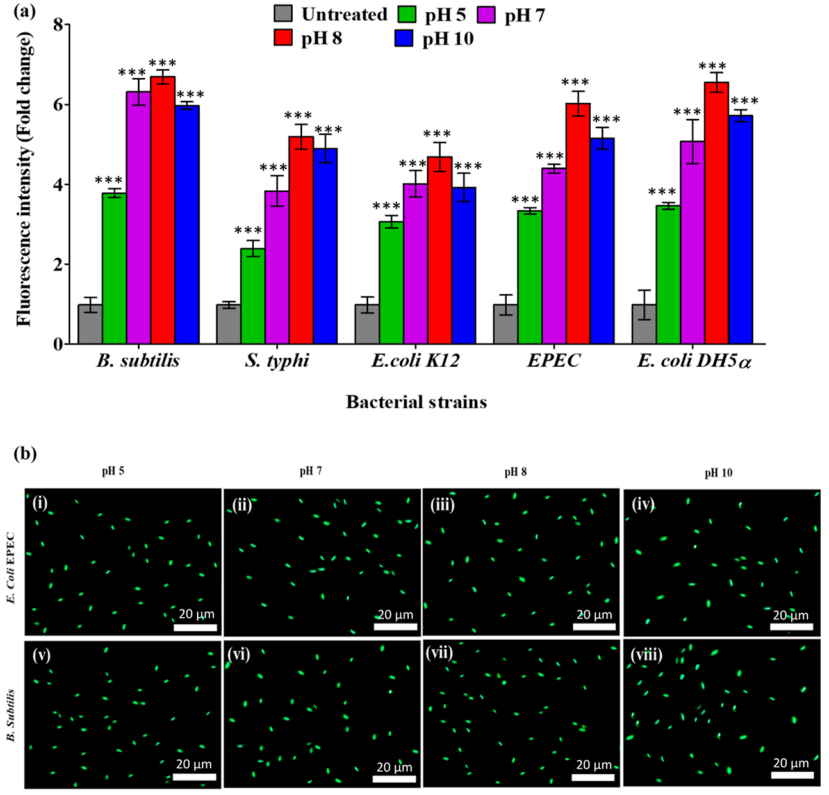

Figure 1. (a) CellTox Green uptake assay. The fluorescence intensity of bacteria treated with bAgNPs was measured at 490 nm using a spectrofluorometer. The values presented are mean ± SE of multiple samples ($N = 3$). The fluorescence intensity of bAgNP-treated bacterial strains was significantly higher than that of untreated bacteria and ***$P < 0.001$. (b) Both EPEC (Gram-negative) and *B. subtilis* RBW (Gram-positive) were treated with bAgNPs synthesized at pH 5 (i,v), 7 (ii,vi), 8 (iii,vii), and 10 (iv,viii). The treated bacteria were then incubated with CellTox green to stain the DNA of the cell wall-compromised bacteria, and green fluorescence was observed under a fluorescence microscope. Scale bar: 20 μm.

change between pH 5 and 10. Hence, solution pH does not significantly influence the ζ potential values of bAgNPs.[49] Overall, our data confirm the role of pH in determining the size, stability, and surface charge of bAgNPs.

3.2. Antimicrobial Activity Assay. *3.2.1. Determination of the ZOI and MIC.* The disk diffusion method was used to investigate the antibacterial propensity of the as-synthesized bAgNPs against Gram-positive (i.e., *B. subtilis*) and Gram-negative bacteria (i.e., *E. coli* DH5α, EPEC, *E. coli* K12, and *S. typhi*) (Table 1). Different concentrations of bAgNPs (i.e., 60, 40, or 20 μg) were used in the antibacterial activity study. The antibacterial activity of the as-synthesized bAgNPs increased consistently against all tested bacterial strains with the increase in nanoparticle dose (Tables S2−S6). The MIC value of bAgNPs against all tested bacteria was 0.125 μg/mL (Table 1). As shown in Table 1, all the bAgNPs synthesized at different pHs (i.e., 5, 7, 8, and 10) exhibited higher antibacterial activity against Gram-positive bacteria (i.e., *B. subtilis*) than Gram-negative bacteria (i.e., *E. coli* DH5α, EPEC, *E. coli* K12, and *S. typhi*). Interestingly, bAgNPs synthesized at pH 8 exhibited the highest antibacterial activity against all the tested bacteria (Table 1). More specifically, the highest antibacterial activity of bAgNPs synthesized at pH 8 was observed against *B. subtilis* (dose: 60 μg), and the area of inhibited zone was 29.5 ± 0.8 mm in diameter. On the other hand, bAgNPs synthesized at pH 8 exhibited the lowest antibacterial activity against *E. coli* K12 and the area of inhibited zone was 11 ± 0 mm in diameter. Both plant extract and $AgNO_3$ exhibited less antibacterial activity when compared to that of bAgNPs. In addition, our as-synthesized bAgNPs exhibited improved antibacterial activity when compared to that of biogenic AgNPs reported in the literature.[14,15,50−52] For instance, the as-

https://doi.org/10.1021/acsomega.2c01922
ACS Omega 2022, 7, 27216−27229

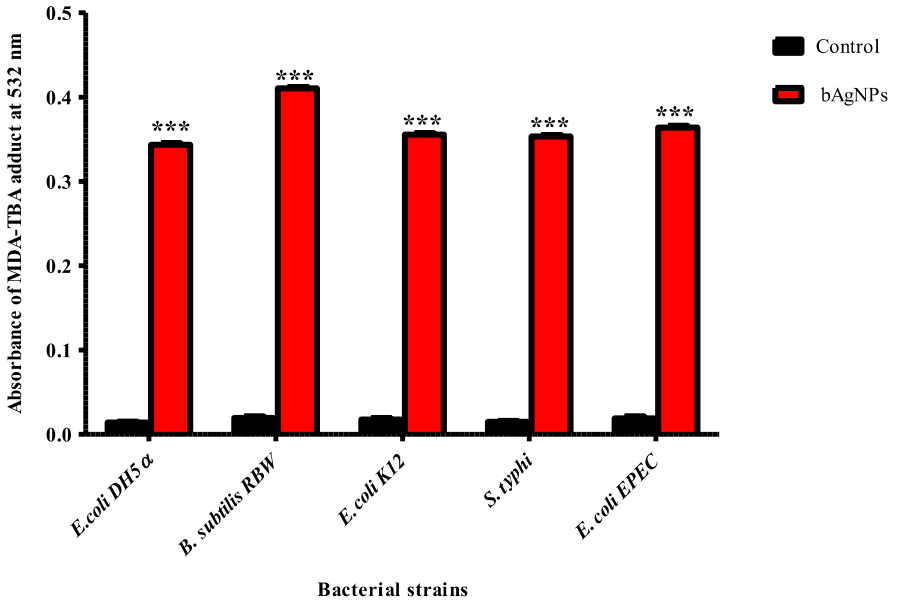

Figure 2. Lipid peroxidation assay. The cell membrane fatty acid oxidation potential of bAgNPs synthesized at pH 8 was measured through malondialdehyde−thiobarbituric acid (MDA−TBA) adduct assay. The absorbance of the MDA−TBA pink adduct was measured at 532 nm. The values presented are mean ± SE of multiple samples ($N = 3$). Data were analyzed using one-way ANOVA followed by Tukey's multiple comparison test. The absorbance of the MDA−TBA adduct of bAgNP-treated bacteria were significantly higher than that of the untreated bacteria (i.e., control) and ***$P < 0.01$.

synthesized bAgNPs synthesized at pH 8 demonstrated lower MIC values[50−52] and a larger ZOI[14,15,52] when compared to that published in the literature.

3.2.2. CellTox Green Assay. The antibacterial activity of the as-synthesized bAgNPs was also confirmed using CellTox green assay. Since CellTox green is a DNA-binding fluorescent dye and is impenetrable to undamaged cells, it is used to identify dead cells.[14] When bAgNP-treated bacteria are incubated with CellTox green dye, the fluorescent dye passes through the compromised bacterial cell membrane and binds to the DNA, resulting in the emission of green fluorescence.[14] Bacterial strains treated with bAgNPs synthesized at pH 8 showed the highest fluorescence intensity (Figure 1a). *B. subtilis* showed the highest fluorescence intensity that is ∼six fold higher than that of the untreated group. The findings are in the same line with those of the area of clear ZOIs (in millimeter) observed in disk diffusion assay. The damage to the bacterial cell membrane was confirmed by the green appearance of dead bacteria under a fluorescence microscope (Figure 1b).

3.2.3. Trypan Blue Dye Assay. Since bAgNPs synthesized at pH 8 showed the maximum antibacterial activity (Figure S4) during disk diffusion assay and CellTox green assay, trypan blue dye exclusion assay was also performed to confirm their bactericidal activity. An intact cell membrane excludes trypan blue dye, while dead cells or membrane compromised cells do not.[14] Therefore, dead or nonviable cells appear blue under a phase-contrast light microscope (Figure S4). The trypan blue dye exclusion assay confirms the highest antibacterial propensity of bAgNPs synthesized at pH 8 against all the tested bacterial strains. The relatively small size of bAgNPs synthesized at pH 8 when compared to others (i.e., bAgNPs synthesized at pH 5, 7, and 10) might be responsible for their greater bactericidal activity. Nanoparticles synthesized at pH 8 have a greater surface area to volume ratio (i.e., 0.349) than that of nanoparticles synthesized at other pH values (i.e., 5, 7, and 10) (Table S7). This is because nanoparticles with smaller size demonstrate better antibacterial activity due to their greater surface-to-volume ratio.[53] *S. cymosum* contains various secondary metabolites including flavonoids and steroids.[21] The conjugation of phytoconstituents with bAgNPs was revealed through FTIR spectroscopy. The negative surface charge of the as-synthesized bAgNPs brought about hydrophobic interactions with bacteria.[14] Furthermore, molecular crowding also plays a crucial role in the interaction between bAgNPs and bacteria.[54] Ag^+ released from bAgNPs interacts with the bacterial cell membrane and results in increased cell membrane permeability.[55] AgNPs or released Ag^+ from bAgNPs also accumulate envelop protein, leading to the enhanced penetration of nanoparticles through cell membranes. Once inside the cells, silver ions either interact with DNA and arrest its replication capability or interact with thiol groups of proteins and inactivate them.[55]

The bAgNPs synthesized at different pHs (i.e., 5, 7, 8, and 10) showed greater antibacterial activity against Gram-positive bacterial strains (i.e., *B. subtilis*) than Gram-negative bacterial strains (i.e., *E. coli* DH5α, EPEC, *E. coli* K12, and *S. typhi*) (Table 1). This can be attributed to the differences in their membrane structure and composition. Different membrane compositions of Gram-positive and Gram-negative bacteria provide distinct pathways for the uptake of nanoparticles.[56] Gram-negative bacterial cell membrane contains lipopolysaccharides (LPSs), phospholipids, and lipoproteins, which are associated with selective penetration barriers for molecules. LPSs are unique to Gram-negative bacteria, which are responsible for the negative charge on the cell membrane. On the other hand, teichoic acid is present only in the cell membrane of Gram-positive bacteria. It also has a thick peptidoglycan layer and numerous pores that permit the penetration of foreign molecules, which causes membrane destabilization, damage, and cellular death. The Gram-positive bacterial cell membrane is more negatively charged than the

https://doi.org/10.1021/acsomega.2c01922
ACS Omega 2022, 7, 27216−27229

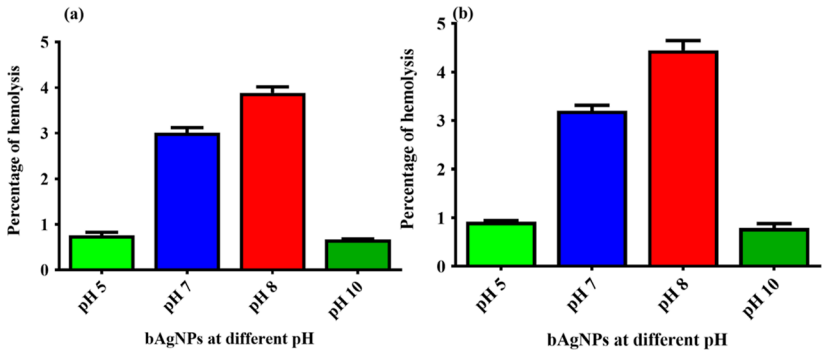

Figure 3. Hemocompatibility assay of bAgNPs synthesized at different pH values against (a) rat RBCs and (b) human RBCs. The values presented are mean ± SE and data and were analyzed using GraphPad Prism 5.0 (GraphPad software) using ANOVA followed by Tukey's multiple comparison test. No statistical significant difference was observed among the different bAgNPs and $p > 0.05$.

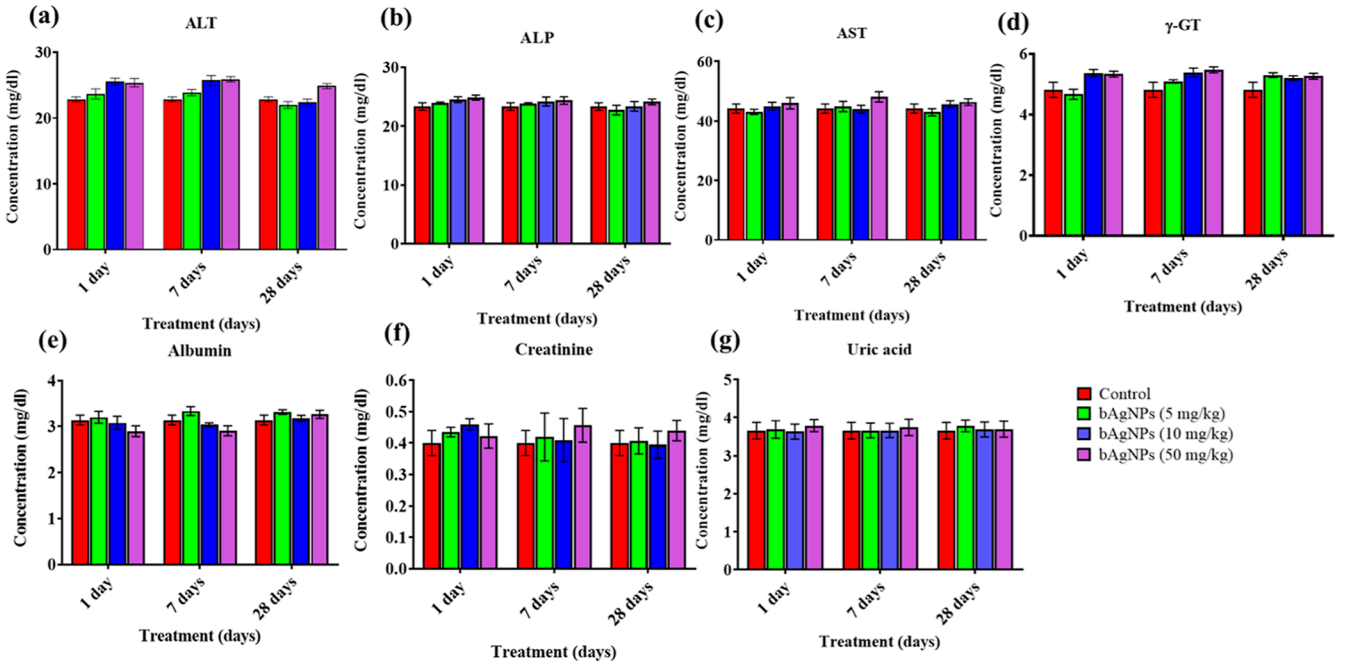

Figure 4. In vivo cytotoxicity assay. The effect of bAgNPs synthesized at pH 8 on the liver was investigated by measuring the level of (a)ALT, (b)ALP, (c)AST, (d)γ-GT, and (e)albumin. Moreover, the effect of bAgNPs on kidney function was also investigated by measuring the level of (f) creatinine and (g) Uric acid. The values presented are mean ± SE, and four animals were taken per group. Data were analyzed using GraphPad Prism 5.0 (GraphPad software) using ANOVA. Dunnett test was used for posthoc comparison. No significant difference was observed when treatment groups were compared with the control and $P > 0.05$.

cell membrane of Gram-negative bacteria.[56] Therefore, bAgNPs interact more efficiently with Gram-positive bacteria via hydrophobic interaction and show higher antibacterial activity. Differences in the bactericidal activity of bAgNPs against particular bacterial strains are attributed to the differences in the chain orientation of the lipid membrane, membrane gross composition, or the presence of specific protein complexes on the bacterial cell wall surface.[57] This result is consistent with the study of Espinosa-Cristobal et al., where they reported that the antibacterial activity of nanoparticles increases as their size reduces.[58] In general, the smaller bAgNPs demonstrate better antibacterial activity. On the other hand, the biocompatibility and the antibacterial activity increases with the decrease in the size of AgNPs.[59] Furthermore, the size of bAgNPs synthesized at pH 8 is the smallest (Figure S1 and Table S7). It has been reported that the smaller AgNPs demonstrate greater bactericidal activity[60,61] due to their large surface area to attach with the bacterial membrane,[60,62] resulting in the increased permeability of the outer membrane. This leads to the increased entry of bAgNPs into the cells[31,63] that brings about bacterial death.

3.3. Lipid Peroxidation Potential Assay. Lipid peroxidation assay is performed to unravel the mechanism of bactericidal propensity of bAgNPs. The bAgNPs exert antibacterial activity through the production of lipid peroxide in the form of the MDA−TBA adduct,[14,26] which prompted us to investigate the lipid peroxidation (i.e., oxidation of the fatty acid of the bacterial cell membrane) potential of bAgNPs synthesized at pH 8 (Figure 2). The release of Ag^+ ions from AgNPs activates the surrounding oxygen molecule that produces free radicals and reactive oxygen species (ROS).[56] Free radicals oxidize bacterial membrane fatty acids and generate malondialdehyde (MDA), which indicates lipid peroxidation. Thus, the concentration of MDA is directly proportional to the amount of ROS produced by bAgNPs. The resulting ROS causes loss of membrane integrity and damage

https://doi.org/10.1021/acsomega.2c01922
ACS Omega 2022, 7, 27216−27229

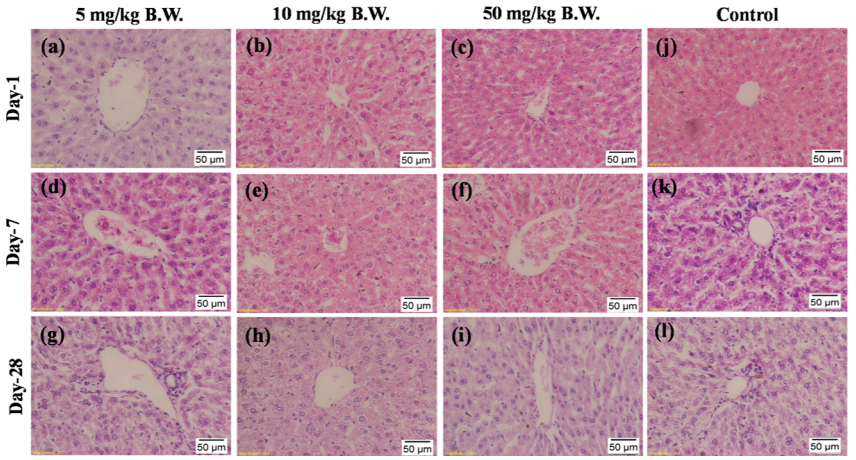

Figure 5. Representative images of histologic changes in liver tissues. All samples prepared from rats were stained with H&E and observed under a light microscope under 20× magnification. (a) bAgNPs at 5 mg/kg B.W at day 1, (b) bAgNPs at 10 mg/kg B.W at day 1, (c) bAgNPs at 50 mg/kg B.W at day 1, (d) bAgNPs at 5 mg/kg B.W at day 7, (e) bAgNPs at 10 mg/kg B.W at day 7, (f) bAgNPs at 50 mg/kg B.W at day 7, (g) bAgNPs at 5 mg/kg B.W at day 28, (h) bAgNPs at 10 mg/kg B.W at day 28, (i) 50 mg/kg B.W at day 28, (j) control group of rats at day 1, (k) control group of rats at day 7, and (l) control group of rats at day 28.

of the bacterial cell membrane and cell structure followed by bacterial growth inhibition.[56,64] Peroxidation of membrane fatty acids enhances membrane permeability, which facilitates the penetration of bAgNPs through the bacterial membrane.[65] Among other tested bacterial strains, the highest amount of the MDA−TBA adduct was observed when Gram-positive bacteria (*B. subtilis*) were treated with bAgNPs synthesized at pH 8. This result is well-correlated with the observation of the highest ZOI and the highest fluorescence intensity obtained through disk diffusion assay and CellTox green assay.

3.4. Biocompatibility Assay. The biocompatibility of nanoparticles has a significant influence on their biomedical applications. Therefore, we investigated their hemocompatibility in vitro and biocompatibility in vivo using the rat model.

3.4.1. In vitro Hemocompatibility Assay. In vitro hemocompatibility of bAgNPs synthesized at different pH values (i.e., 5, 7, 8, and 10) was investigated using rat and human RBCs. The highest bactericidal dose (i.e., 60 μg) of all the as-synthesized bAgNPs was used to investigate the hemolytic potential. All the bAgNPs exhibited negligible hemolytic potential (i.e., less than 5%) against both rat and human RBCs (Figure 3). More precisely, bAgNPs synthesized at pH 8 showed 4.59 and 4% hemolytic propensity against rat and human RBCs, respectively, which is well below the acceptable value (i.e., up to 5%) for the clinical applications of nanoparticles according to World Health Organization (WHO) guidelines. The excellent hemocompatibility of bAgNPs is attributed to their negative ζ potential (Table S1) that generates electrostatic repulsion with the negatively charged RBCs. The percentage of hemolysis differ significantly in human and rat RBCs because of the difference in the composition of RBCs' membrane.[14] In addition, we observed that smaller nanoparticles demonstrate high hemocompatibility due to their easy transportability, which supports the data obtained by Nasar, M. Q. et. al.[66] According to the criterion in the ASTM E2524-08 standard, percentage hemolysis <5% indicates that our test nanoparticles cause no significant damage to RBCs.[45]

3.4.2. In vivo Biocompatibility Assay. 3.4.2.1. Organ Function Biomarkers. An in vivo rat model was used to evaluate the biocompatibility of the as-synthesized bAgNPs. The bAgNPs exhibiting the highest antimicrobial activity (synthesized at pH 8) were administered to male Wister rats through the intravenous route in three different doses (5, 10, and 50 mg/kg) and at three different time points (i.e., 1, 7, and 28 days). The biochemical investigation was conducted to examine the damage to liver and kidney tissues by measuring the level of relevant enzymes. The intravenous administration of different concentrations of bAgNPs did not show any statistically significant difference ($P > 0.05$) in liver function biomarkers (i.e., ALT, AST, ALP, γ-GT, and albumin) when compared to the control group (bAgNP-untreated rats) up to 28 days (Figure 4). This observation supports the findings of Kim, Eunjoo, et al., where they showed that intravenous administration of 50−90 nm size AgNPs (dose: 5 mg/kg) for 7 and 28 days exhibits no significant change in the serum ALT and AST level.[67] However, Tiwari, D. K. et al. reported that intravenous administration of AgNPs (dose: >20 mg/kg) increases the serum ALT and AST level, whereas 4 and 10 mg/kg doses do not have any significant impact on serum the ALT and AST level.[68] AgNPs damage liver tissues by generation of ROS.[69] *S. cymosum* contains phenolic acids (e.g., benzoic acid and salicylic acid) and flavonoids (rutin) that possess free radical-scavenging ability. Thus, bAgNPs synthesized using *S. cymosum* leaf extracts maintain the level of serum ALT and AST. *S. cymosum* also plays an important role in restoring the level of serum albumin of the malfunctioned liver.[21] Moreover, the level of serum kidney function biomarkers (i.e., creatinine and uric acid) was also estimated to assess the impact of bAgNPs on renal health. Intravenous administration of three different doses (i.e., 5, 10, and 50 mg/kg) of bAgNPs at three different time points (i.e., 1, 7, and 28 days) did not cause any significant change ($P > 0.05$) in the kidney function biomarkers (Figure 4). We further investigated the lipid profile of rats administered with three different doses (i.e., 5, 10, and 50 mg/kg) of bAgNPs at three different time points (i.e., 1, 7, and 28 days) and observed no significant impact on the lipid profile (e.g., TC, TG, HDL-C, and LDL-C) when compared to the control group (Figure S5). *S. cymosum* extract helps to maintain the lipid profile by lowering TG and TC (total cholesterol) levels while improving the HDL-C level.[21] These findings support the biocompatibility of our as-

https://doi.org/10.1021/acsomega.2c01922
ACS Omega 2022, 7, 27216−27229

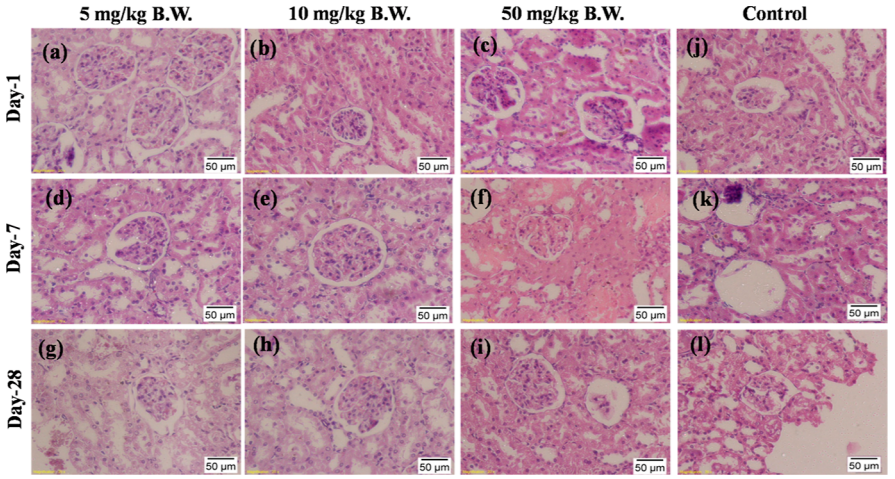

Figure 6. Representative images of histologic changes in kidney tissues. All samples prepared from rats were stained with H&E and observed under a light microscope under 20× magnification. (a) bAgNPs at 5 mg/kg B.W at day 1, (b) bAgNPs at 10 mg/kg B.W at day 1, (c) bAgNPs at 50 mg/kg B.W at day 1, (d) bAgNPs at 5 mg/kg B.W at day 7, (e) bAgNPs at 10 mg/kg B.W at day 7, (f) bAgNPs at 50 mg/kg B.W at day 7, (g) bAgNPs at 5 mg/kg B.W at day 28, (h) bAgNPs at 10 mg/kg B.W at day 28, (i) bAgNPs at 50 mg/kg B.W at day 28, (j) control group of rats at day 1, (k) control group of rats at day 7, and (l) control group of rats at day 28.

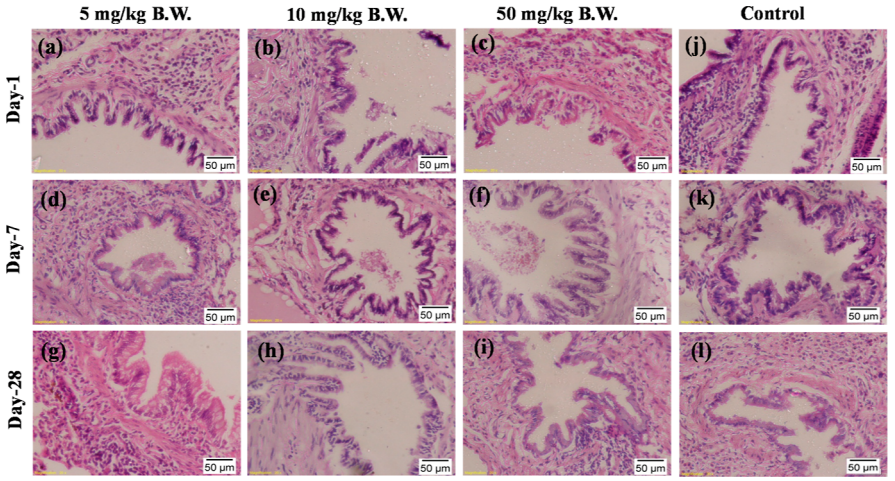

Figure 7. Representative images of histologic changes in lung tissues. All samples prepared from rats were stained with H&E and observed under a light microscope under 20× magnification. (a) bAgNPs at 5 mg/kg B.W at day 1, (b) bAgNPs at 10 mg/kg B.W at day 1, (c) bAgNPs at 50 mg/kg B.W at day 1, (d) bAgNPs at 5 mg/kg B.W at day 7, (e) bAgNPs at 10 mg/kg B.W at day 7, (f) bAgNPs at 50 mg/kg B.W at day 7, (g) bAgNPs at 5 mg/kg B.W at day 28, (h) bAgNPs at 10 mg/kg B.W at day 28, (i) bAgNPs at 50 mg/kg B.W at day 28, (j) control group of rats at day 1, (k) control group of rats at day 7, and (l) control group of rats at day 28.

synthesized bAgNPs. The possible reason of the excellent biocompatibility of bAgNPs is attributed to the presence of various phytochemicals (e.g., alkaloids, carbohydrates, flavonoids, and tannins) found in *S. cymosum* leaf extract.[21]

3.4.2.2. Histopathological Assessment. The toxicity of the as-synthesized bAgNPs was further investigated by histopathological analysis of different vital organs including the liver, kidneys, lungs, spleen, heart, and brain of the experimental rats. To evaluate the toxicity, we performed intravenous administration of bAgNPs rather than oral gavage since oral administration causes poor absorption of AgNPs in the gastrointestinal (GI) tract, resulting in the low bioavailability of nanoparticles in the blood and an excess level of AgNPs in the feces.[70] The bioavailability of AgNPs was only 4.2% when 10 mg/kg nanoparticles were administered through the oral route.[71] On the other hand, intravenous administration of AgNPs (size: 20 nm) helps to effectively cross the cellular barriers of the lungs and GI tract. As a result, the whole dose of nanoparticles is available in the systemic circulation, making them suitable to assess their toxicity, if any, using the benchmark approaches.[72] Furthermore, the concentration of nanoparticles also remain very low in feces when compared to oral administration.[71] A single dose of intravenous administration was administered since multiple doses have been reported to generate toxicity.[69] In addition, no death was reported after single intravenous injection of citrate-coated AgNPs.[70] After intravenous administration through the tail vein, bAgNPs were rapidly cleared off the blood and distributed to different organs of the body. The main target organs for the accumulation of bAgNPs are the spleen, liver, lungs, and kidneys.[69,70] However, small particles (size: 20 nm), similar to the size of our bAgNP synthesized at pH 8, are reported to be accumulated mainly in the liver followed by kidneys and spleen.[73]

Figures 5−7 and S6−S8 represent the histopathological assessments of the liver, kidney, lung, heart, brain, and spleen

https://doi.org/10.1021/acsomega.2c01922
ACS Omega 2022, 7, 27216−27229

sections of experimental rats. Different doses (i.e., 5, 10, and 50 mg/kg) of bAgNPs were intravenously administered at different time points (i.e., 1, 7, and 28 days) to observe their effects on organ histoarchitecture. There was no sign of damage to the hepatic tissue of the treatment groups when compared to the control group (Figure 5). Precisely, hydropic degradation around the central vein (CV), necrosis of hepatocytes, hyperemia, and fibrotic lesions in liver tissue were not observed in any of the treatment groups. However, accumulation of bAgNPs in the hepatic tissue was observed that increased slightly with the increasing dose concentration (i.e., 10 and 50 mg/kg B.W.) of bAgNPs (Figure 5). The accumulated bAgNPs in the CV of hepatocytes decreased after 28 days of administration. This result matches with the previous studies, where accumulation of bAgNPs (7−80 nm) usually reduced after 14−17 days and declined bAgNP deposition was exhibited after 28 days.[70] However, regardless of the accumulation of bAgNPs, no hepatocellular destruction was noticed, which is attributed to the presence of plant phytoconstituents. AgNPs bring about organ toxicity when intracellular ROS elevation surpasses the cellular antioxidant defense mechanism by oxidizing glutathione and protein-bound sulfhydryl groups and induces oxidative stress.[69] *S. cymosum* contains phenolic compounds and flavonoids that have redox potentials to neutralize free radicals by donating hydrogen or electrons, thereby scavenging the generation of free radicals during oxidative stress.[20] Administration of *S. cymosum* leaf extract helps to ameliorate severe disruption of the cellular arrangement, vascular congestion, degeneration of hepatocytes in the peripheral area of the CV associated with inflammatory infiltrates, necrosis of the hepatocytes, and edema at different locations of the lobule.[21] Furthermore, elevated levels of ALT and AST indicate the necrosis of hepatic cells, the albumin level states the functional capability or secretory ability of the liver, and the level of ALP increases upon loss of hepatic membrane integrity.[15] There was no statistically significant elevation of the level of liver function biomarkers (i.e., ALT, AST, ALP, γ-GT, and albumin) (Figure 4) upon administration of different doses of bAgNPs, irrespective of the incubation time. Furthermore, there was no significant increase in the level of serum cholesterol, TG, LDL-C, and HDL-C, (Figure S5) which confirms a low risk of coronary heart disease from the as-synthesized bAgNPs.

Furthermore, undamaged glomerulus along with no swelling and hydropic degeneration of the epithelial cells of proximal tubules were evident under microscopic observation of the kidney tissues after treatment with different doses of bAgNPs for different time points (Figure 6). This confirms normal renal function of the treatment groups. According to Ashajyothi, C et al., 11−75 nm size biogenic AgNPs can be excreted from the body by the kidneys without causing any harm.[74] Conversely, 10 nm-size particles are deleterious for the kidneys.[70] On the other hand, microscopic observation of heart tissue revealed no sign of congestion of heart muscle, extravasation of RBCs, muscle fascicles, and infiltration of immune cells in treatment groups (Figure S6). The signs of lung toxicity such as alveolar wall thickening and the infiltration of focal inflammatory cells[75] were absent in the histopathological images (Figure 7). Moreover, no abnormalities in the brain and spleen tissue were visible in the treatment groups when compared to the control (Figures S7 and S8).

Histological sections demonstrated the clearance of bAgNPs through hepatic, renal, and cardiac circulation, except for brain circulation, and the concentration of the nanoparticles gradually decreased with the progression of time (Figures 5, 6, S6, and S7). Therefore, a dose of 5, 10, and 50 mg/kg B.W. does not cause potential harm to liver, kidney, heart, lung, brain, and spleen tissues.

Apart from the phytoconstituents, the excellent biocompatibility of our bAgNPs can also be attributed to other important parameters. Among others, the size of our as-synthesized bAgNPs is suitable for in vivo studies since it is well established that the toxicity of nanoparticles largely depends on the particle size. For example, small-size ($\leq$10 nm) nanoparticles are found to be toxic.[72] Another important factor for biocompatibility is the presence of biogenic coating around the nanoparticles. Uncoated nanoparticles exert significant toxicity to human whereas particles coated with carbon are nontoxic. This is because carbon coating reduces the direct contact between the particle surface and the cellular constituents.[76] The presence of carbon in the as-synthesized bAgNPs was confirmed by FTIR analysis. Taken together, the excellent biocompatibility in terms of serum biochemical markers and histopathological features of important tissues suggest that bAgNPs are therapeutically safe to administer through the intravenous route at a dose up to 50 mg/kg B.W.

4. CONCLUSIONS

S. cymosum leaf extract was used as a reducing and capping agent to synthesize bAgNPs at different pH values (i.e., 5, 7, 8, and 10). The generation of bAgNPs was confirmed through UV−visible, FTIR, and XRD spectroscopy and TEM. All the bAgNPs were negatively charged because of the conjugation of various phytoconstituents present in the *S.cymosum* leaf extract. The bAgNPs synthesized at pH 8 exhibited the highest antibacterial activity against all the tested bacterial strains through the generation of ROS upon oxidation of membrane fatty acids. More precisely, bAgNPs synthesized at pH 8 demonstrated the highest antibacterial propensity against *B. subtilis* (Gram-positive bacteria). Furthermore, the as-synthesized bAgNPs showed excellent hemocompatibility against rat and human RBCs. Biogenic AgNPs also demonstrated excellent in vivo biocompatibility in terms of liver and kidney function biomarkers (i.e., serum ALT, AST, ALP, γ-GT, albumin, creatinine, and uric acid). Histopathological assessment of liver, kidneys, lungs, spleen, heart, and brain tissues also confirm the biocompatibility of the as-synthesized bAgNPs. Hence, bAgNPs could be subjected to further clinical investigations before using as a suitable alternative to commercially available antimicrobial agents.

■ ASSOCIATED CONTENT

Supporting Information

The Supporting Information is available free of charge at https://pubs.acs.org/doi/10.1021/acsomega.2c01922.

Ultraviolet−visible absorption spectra; scanning TEM images of bAgNPs synthesized at pH 5, 7, 8, and 10; FTIR spectra of plant extract, silver nitrate, and bAgNPs synthesized at four different pH values (i.e., pH 5, 7, 8, and 10); powder XRD analysis of the as-synthesized bAgNPs synthesized at pH 5, 7, 8, and 10; hydrodynamic diameter, polydispersity index (PDI), and ζ potential of bAgNPs; antibacterial activity of the as-synthesized bAgNPs against *B. subtilis*, *E. coli* DH5α, *E. coli* k12, EPEC, and *S. typhi* in different doses and at

https://doi.org/10.1021/acsomega.2c01922
ACS Omega 2022, 7, 27216−27229

different time points; trypan blue dye exclusion assay to investigate the bactericidal effect of bAgNPs synthesized at pH 8 against different bacterial strains (i.e., *B. subtilis*, E. coli DH5α, E. coli K12, EPEC, and *S. typhi*); detailed information about the calculation of surface to volume ratios of bAgNPs at four different pH values (i.e., pH 5, 7, 8, and 10); investigation of the effect of bAgNPs synthesized at pH 8 on biochemical parameters; representative images of histologic changes in heart tissues, brain tissues, and spleen tissues; qualitative estimation of the phytochemical constituents of *S. cymosum*; and antibacterial activity of povidone iodine against experimental bacterial strains at 12 h (PDF)

AUTHOR INFORMATION

Corresponding Authors

Md. Ashraful Hasan − *Department of Biochemistry and Molecular Biology, Jahangirnagar University, Dhaka 1342, Bangladesh*; Phone: +8801933123455; Email: ashrafulhasan@juniv.edu

Satya Ranjan Sarker − *Department of Biotechnology and Genetic Engineering, Jahangirnagar University, Dhaka 1342, Bangladesh*; orcid.org/0000-0001-7015-6834; Phone: +8801310765603; Email: satya.sarker@bgeju.edu.bd

Authors

Kazi Mustafa Mahmud − *Department of Biochemistry and Molecular Biology, Jahangirnagar University, Dhaka 1342, Bangladesh*

Md. Monir Hossain − *Department of Biotechnology and Genetic Engineering, Jahangirnagar University, Dhaka 1342, Bangladesh*; orcid.org/0000-0003-0749-9994

Shakil Ahmed Polash − *Department of Biotechnology and Genetic Engineering, Jahangirnagar University, Dhaka 1342, Bangladesh; Nano Biotechnology Research Laboratory (NBRL), School of Science, RMIT University, Melbourne, Victoria 3001, Australia*

Masato Takikawa − *Department of Advanced Science and Engineering, Waseda University (TWIns), Shinju-ku, Tokyo 162-8480, Japan*; orcid.org/0000-0003-4856-9717

Md Salman Shakil − *Department of Biochemistry and Molecular Biology, Jahangirnagar University, Dhaka 1342, Bangladesh; Department of Mathematics and Natural Sciences, Brac University, Dhaka 1212, Bangladesh*; orcid.org/0000-0002-8922-9500

Md Forhad Uddin − *Department of Biochemistry and Molecular Biology, Jahangirnagar University, Dhaka 1342, Bangladesh*

Morshed Alam − *Department of Biochemistry and Molecular Biology, Jahangirnagar University, Dhaka 1342, Bangladesh*

Mohammad Mahfuz Ali Khan Shawan − *Department of Biochemistry and Molecular Biology, Jahangirnagar University, Dhaka 1342, Bangladesh*

Tanushree Saha − *Department of Textile Engineering, Dhaka University of Engineering and Technology, Gazipur 1707, Bangladesh; School of Engineering, RMIT University, Melbourne, Victoria 3001, Australia*

Shinji Takeoka − *Department of Life Science and Medical Bioscience, Graduate School of Advance Science and Engineering, Waseda University (TWIns), Shinju-ku, Tokyo 162-8480, Japan*; orcid.org/0000-0002-6230-1517

Complete contact information is available at: https://pubs.acs.org/10.1021/acsomega.2c01922

Author Contributions

K.M.M. and M.M.H. have contributed equally to this work. All authors contributed in the experimental, analysis, and article preparation.

Notes

The authors declare no competing financial interest.

ACKNOWLEDGMENTS

The project was partially supported by Jahangirnagar University research grant 2018, Govt. Of Bangladesh. The authors thank the Wazed Mia Science Research Centre (WMSRC), Jahangirnagar University, for allowing their facilities to characterize the nanoparticles. The authors also thank the Waseda University Central Instrument Facility, Tokyo, Japan, for allowing their comprehensive facilities and services.

REFERENCES

(1) Shirali, G. S.; Pazhayattil, A. C. Drug-induced impairment of renal function. *Int. J. Nephrol. Renovasc. Dis.* **2014**, *7*, 457.

(2) Mohsen, S.; Dickinson, J. A.; Somayaji, R. Update on the adverse effects of antimicrobial therapies in community practice. *Am. Fam. Physician* **2020**, *66*, 651−659.

(3) Robles, M.; Toscano, E.; Cotta, J.; Isabel Lucena, M.; Andrade, R. J. Antibiotic-induced liver toxicity: mechanisms, clinical features and causality assessment. *Curr. Drug Saf.* **2010**, *5*, 212−222.

(4) Roco, M. C. The long view of nanotechnology development: the National Nanotechnology Initiative at 10 years. In *Nanotechnology Research Directions for Societal Needs in 2020*; SpringerScience Policy Reports; Springer, 2010, pp 1−28.

(5) Zhang, X.-F.; Liu, Z.-G.; Shen, W.; Gurunathan, S. Silver nanoparticles: synthesis, characterization, properties, applications, and therapeutic approaches. *Int. J. Mol. Sci.* **2016**, *17*, 1534.

(6) Burduşel, A.-C.; Gherasim, O.; Grumezescu, A. M.; Mogoantă, L.; Ficai, A.; Andronescu, E. J. N. Biomedical applications of silver nanoparticles: an up-to-date overview. *Nanomaterials* **2018**, *8*, 681.

(7) Khorrami, S.; Zarrabi, A.; Khaleghi, M.; Danaei, M.; Mozafari, M. Selective cytotoxicity of green synthesized silver nanoparticles against the MCF-7 tumor cell line and their enhanced antioxidant and antimicrobial properties. *Int. J. Nanomed.* **2018**, *Volume 13*, 8013.

(8) Alsammarraie, F. K.; Wang, W.; Zhou, P.; Mustapha, A.; Lin, M. J. C.; Biointerfaces, S. B. Green synthesis of silver nanoparticles using turmeric extracts and investigation of their antibacterial activities. *Colloids Surf., B* **2018**, *171*, 398−405.

(9) Roy, A.; Bulut, O.; Some, S.; Mandal, A. K.; Yilmaz, M. D. Green synthesis of silver nanoparticles: biomolecule-nanoparticle organizations targeting antimicrobial activity. *RSC Adv.* **2019**, *9*, 2673−2702.

(10) Jain, D.; Daima, H. K.; Kachhwaha, S.; Kothari, S. L. Synthesis of plant-mediated silver nanoparticles using papaya fruit extract and evaluation of their anti microbial activities. *Dig. J. Nanomater. Biostruct.* **2009**, *4*, 557−563.

(11) Traiwatcharanon, P.; Timsorn, K.; Wongchoosuk, C. J. Flexible room-temperature resistive humidity sensor based on silver nanoparticles. *Mater. Res. Express* **2017**, *4*, 085038.

(12) Hamouda, R. A.; Hussein, M. H.; Abo-elmagd, R. A.; Bawazir, S. S. Synthesis and biological characterization of silver nanoparticles derived from the cyanobacterium Oscillatoria limnetica. *Sci. Rep.* **2019**, *9*, No. 13071.

(13) Polash, S. A.; Hossain, M. M.; Saha, T.; Sarker, S. R. Biogenic Silver Nanoparticles: A Potent Therapeutic Agent. In *Emerging Trends in Nanomedicine*; Singh, S., Ed.; Springer: Singapore, 2021; pp 81−127. DOI: 10.1007/978-981-15-9920-0_4.

(14) Hossain, M.; Polash, S. A.; Takikawa, M.; Shubhra, R. D.; Saha, T.; Islam, Z.; Hossain, S.; Hasan, M.; Takeoka, S.; Sarker, S. R. J.

biotechnology, Investigation of the antibacterial activity and in vivo cytotoxicity of biogenic silver nanoparticles as potent therapeutics. *Front. Bioeng. Biotechnol.* **2019**, *7*, 239.
(15) Niloy, M. S.; Hossain, M. M.; Takikawa, M.; Shakil, M. S.; Polash, S. A.; Mahmud, K. M.; Uddin, M. F.; Alam, M.; Shubhra, R. D.; Shawan, M. M. A. K. J. A. A. B. M.; Saha, T.; Takeoka, S.; Hasan, M. A.; Ranjan Sarker, S. Synthesis of Biogenic Silver Nanoparticles Using Caesalpinia digyna and Investigation of Their Antimicrobial Activity and In Vivo Biocompatibility. *ACS Appl. Bio Mater.* **2020**, *3*, 7722−7733.
(16) Valdivieso-Ugarte, M.; Gomez-Llorente, C.; Plaza-Díaz, J.; Gil, Á. J. N. Antimicrobial, antioxidant, and immunomodulatory properties of essential oils: A systematic review. *Nutrients* **2019**, *11*, 2786.
(17) Park, M.-J.; Gwak, K.-S.; Yang, I.; Choi, W.-S.; Jo, H.-J.; Chang, J.-W.; Jeung, E.-B.; Choi, I.-G. Antifungal activities of the essential oils in Syzygium aromaticum (L.) Merr. Et Perry and Leptospermum petersonii Bailey and their constituents against various dermatophytes. *J. Microbiol.* **2007**, *45*, 460−5.
(18) Hossainey, M. R. H.; Sazed, S. A.; Nima, M. K.; Rahman, M. S.; Ashraf, T.; Chowdhury, A. A.; Rashid, M. A.; Haque, R.; Alam, M. S. Investigation of antimalarial activity and cytotoxicity profiling of a Bangladeshi plant Syzygium cymosum. *J. Infect. Dev. Countries* **2020**, *14*, 924−928.
(19) Paiva, P. M. G.; Gomes, F. S.; Napoleão, T. H.; Sá, R. A.; Correia, M. T. S.; Coelho, L. C. B. Antimicrobial activity of secondary metabolites and lectins from plants. In *Current Research, Technology and Education Topics in Applied Microbiology and Microbial Biotechnology*; Méndez-Vilas, A. Ed.; Formatex Research Center, Bajadoz, Spain, 2010; pp 396−406.
(20) Dhar, K. S.; Wahed, T. B.; Hasan, A. N. M.; Wahed, S. B. In vitro antioxidant activities and cytotoxicity study of the methanolic extract of barks of Syzygium cymosum. *Int. J. Pharmaceut. Res. Allied Sci.* **2016**, *7*, 1021.
(21) Wahed, T. B.; Mondal, M.; Rahman, M. A.; Hossen, M. S.; Bhoumik, N. C.; Saha, S.; Tanvir, E.; Khalil, M. I.; Kundu, S. K.; Islam, M. T. J. C. r. i. t.; Mubarak, M. S. Protective role of Syzygium Cymosum leaf extract against carbofuran-induced hematological and hepatic toxicities. *Chem. Res. Toxicol.* **2019**, *32*, 1619−1629.
(22) Khandel, P.; Yadaw, R. K.; Soni, D. K.; Kanwar, L.; Shahi, S. K. Biogenesis of metal nanoparticles and their pharmacological applications: present status and application prospects. *J. Nanostruct. Chem.* **2018**, *8*, 217−254.
(23) Ahmed, S.; Saifullah; Ahmad, M.; Swami, B. L.; Ikram, S. J. Green synthesis of silver nanoparticles using Azadirachta indica aqueous leaf extract. *J. Radiat. Res. Appl. Sci.* **2016**, *9*, 1−7.
(24) Mondal, R.; Polash, S. A.; Saha, T.; Islam, Z.; Sikder, M. M.; Alam, N.; Hossain, M. S.; Sarker, S. R. Investigation of the Phytoconstituents and Bioactivity of Various Parts of Wild Type and Cultivated *Phyllanthus emblica* L. *Adv. Biosci. Biotechnol.* **2017**, *08*, 211.
(25) Polash, S. A.; Saha, T.; Hossain, M. S.; Sarker, S. R. Investigation of the Phytochemicals, Antioxidant, and Antimicrobial Activity of the *Andrographis paniculata* Leaf and Stem Extracts. *Adv. Biosci. Biotechnol.* **2017**, *08*, 149.
(26) Ranjan Sarker, S.; Polash, S. A.; Boath, J.; Kandjani, A. E.; Poddar, A.; Dekiwadia, C.; Shukla, R.; Sabri, Y.; Bhargava, S. K. J. Functionalization of elongated tetrahexahedral Au nanoparticles and their antimicrobial activity assay. *ACS Appl. Mater. Interfaces* **2019**, *11*, 13450−13459.
(27) Zhang, J.-H.; Chung, T. D.; Oldenburg, K. R. J. A simple statistical parameter for use in evaluation and validation of high throughput screening assays. *J. Biomol. Screening* **1999**, *4*, 67−73.
(28) Lee, J. H.; Gulumian, M.; Faustman, E. M.; Workman, T.; Jeon, K.; Yu, I. J. J. Blood biochemical and hematological study after subacute intravenous injection of gold and silver nanoparticles and coadministered gold and silver nanoparticles of similar sizes. *BioMed Res. Int.* **2018**, *2018*, 8460910.
(29) Raja, P. B.; Rahim, A. A.; Qureshi, A. K.; Awang, K. Green synthesis of silver nanoparticles using tannins. *Mater. Sci.* **2014**, *32*, 408−413.
(30) Ahmed, T.; Ogulata, R. T. J. A Review on Silver Nanoparticles—Green Synthesis, Antimicrobial Action and Application in Textiles. *J. Nat. Fibers* **2021**, *2021*, 1−22.
(31) Li, W.-R.; Xie, X.-B.; Shi, Q.-S.; Zeng, H.-Y.; OU-Yang, O.-Y.; Chen, Y.-B. Antibacterial activity and mechanism of silver nanoparticles on Escherichia coli. *Appl. Microbiol. Biotechnol.* **2010**, *85*, 1115−1122.
(32) Ahluwalia, V.; Elumalai, S.; Kumar, V.; Kumar, S.; Sangwan, R. S. Nano silver particle synthesis using Swertia paniculata herbal extract and its antimicrobial activity. *Microb. Pathog.* **2018**, *114*, 402−408.
(33) Zuorro, A.; Iannone, A.; Natali, S.; Lavecchia, R. J. P. Green synthesis of silver nanoparticles using bilberry and red currant waste extracts. *Processes* **2019**, *7*, 193.
(34) Ranjani, B.; Pandian, K.; Kumar, G. A.; Gopinath, S. J. D-glucosamine chitosan base molecule-assisted synthesis of different shape and sized silver nanoparticles by a single pot method: A greener approach for sensor and microbial applications. *Int. J. Biol. Macromol.* **2019**, *133*, 1280−1287.
(35) Alqadi, M.; Abo Noqtah, O.; Alzoubi, F.; Alzouby, J.; Aljarrah, K. J. pH effect on the aggregation of silver nanoparticles synthesized by chemical reduction. *Mater. Sci.* **2014**, *32*, 107−111.
(36) Axson, J. L.; Stark, D. I.; Bondy, A. L.; Capracotta, S. S.; Maynard, A. D.; Philbert, M. A.; Bergin, I. L.; Ault, A. P. Rapid kinetics of size and pH-dependent dissolution and aggregation of silver nanoparticles in simulated gastric fluid. *J. Phys. Chem. C* **2015**, *119*, 20632−20641.
(37) Attallah, N. G.; Elekhnawy, E.; Negm, W. A.; Hussein, I. A.; Mokhtar, F. A.; Al-Fakhrany, O. M. In vivo and in vitro antimicrobial activity of biogenic silver nanoparticles against Staphylococcus aureus clinical isolates. *Pharmaceuticals* **2022**, *15*, 194.
(38) Das, G.; Shin, H.-S.; Patra, J. K. Multitherapeutic Efficacy of Curly Kale Extract Fabricated Biogenic Silver Nanoparticles. *Int. J. Nanomed.* **2022**, *17*, 1125.
(39) Ranoszek-Soliwoda, K.; Tomaszewska, E.; Małek, K.; Celichowski, G.; Orlowski, P.; Krzyzowska, M.; Grobelny, J. J. C.; Biointerfaces, S. B. The synthesis of monodisperse silver nanoparticles with plant extracts. *Colloids Surf., B* **2019**, *177*, 19−24.
(40) Zubair, M.; Azeem, M.; Mumtaz, R.; Younas, M.; Adrees, M.; Zubair, E.; Khalid, A.; Hafeez, F.; Rizwan, M.; Ali, S. J. Green synthesis and characterization of silver nanoparticles from Acacia nilotica and their anticancer, antidiabetic and antioxidant efficacy. *Environ. Pollut.* **2022**, *304*, 119249.
(41) Ghetas, H. A.; Abdel-Razek, N.; Shakweer, M. S.; Abotaleb, M. M.; Ahamad Paray, B. A.; Ali, S.; Eldessouki, E. A.; Dawood, M. A.; Khalil, R. H. Antimicrobial activity of chemically and biologically synthesized silver nanoparticles against some fish pathogens. *Saudi J. Biol. Sci.* **2022**, *29*, 1298−1305.
(42) Janakiraman, N.; Johnson, M. J. Functional groups of tree ferns (Cyathea) using FTIR: Chemotaxonomic implications. *Rom. J. Biophys.* **2015**, *25*, 131−141.
(43) Zhuang, J.; Li, M.; Pu, Y.; Ragauskas, A. J.; Yoo, C. G. Observation of potential contaminants in processed biomass using fourier transform infrared spectroscopy. *Appl. Sci.* **2020**, *10*, 4345.
(44) Bershtein, V.; Gun'ko, V.; Egorova, L.; Guzenko, N.; Pakhlov, E.; Ryzhov, V.; Zarko, V. Well-Defined Oxide Core-Poly(vinyl pyrrolidone) Shell Nanoparticles: Interactions and Multi-Modal Glass Transition Dynamics at Interfaces. *Macromol. Symp.* **2010**, *296*, 541−549.
(45) Nayak, D.; Kumari, M.; Rajachandar, S.; Ashe, S.; Thathapudi, N. C.; Nayak, B. Biofilm impeding AgNPs target skin carcinoma by inducing mitochondrial membrane depolarization mediated through ROS production. *ACS Appl. Mater. Interfaces* **2016**, *8*, 28538−28553.
(46) Khan, M. J.; Shameli, K.; Sazili, A. Q.; Selamat, J.; Kumari, S. J. Rapid green synthesis and characterization of silver nanoparticles

https://doi.org/10.1021/acsomega.2c01922
ACS Omega 2022, 7, 27216−27229

arbitrated by curcumin in an alkaline medium. *Molecules* **2019**, *24*, 719.
(47) Rao, K. J.; Paria, S. Aegle marmelos Leaf Extract and Plant Surfactants Mediated Green Synthesis of Au and Ag Nanoparticles by Optimizing Process Parameters Using Taguchi Method. *ACS Sustainable Chem. Eng.* **2015**, *3*, 483−491.
(48) Gontijo, L. A. P.; Raphael, E.; Ferrari, D. P. S.; Ferrari, J. L.; Lyon, J. P.; Schiavon, M. pH effect on the synthesis of different size silver nanoparticles evaluated by DLS and their size-dependent antimicrobial activity. *Matéria (Rio J.)* **2020**, *25*, No. e-12846.
(49) Lau, C. P.; Abdul-Wahab, M. F.; Jaafar, J.; Chan, G. F.; Rashid, N. A. A. Effect of pH and biological media on polyvinylpyrrolidone-capped silver nanoparticles. *AIP Conf. Proc.* **2016**, *1756*, No. 080002.
(50) Aref, M. S.; Salem, S. Bio-callus synthesis of silver nanoparticles, characterization, and antibacterial activities via Cinnamomum camphora callus culture. *Biocatal. Agric. Biotechnol.* **2020**, *27*, 101689.
(51) Sengupta, A.; Sarkar, A. Synthesis and characterization of nanoparticles from neem leaves and banana peels: a green prospect for dye degradation in wastewater. *Ecotoxicology* **2021**, *31*, 537−548.
(52) Sharifi-Rad, M.; Pohl, P.; Epifano, F. Phytofabrication of silver nanoparticles (Agnps) with pharmaceutical capabilities using otostegia persica (burm.) boiss. leaf extract. *Nanomaterials* **2021**, *11*, 1045.
(53) Qasim, M.; Udomluck, N.; Chang, J.; Park, H.; Kim, K. Antimicrobial activity of silver nanoparticles encapsulated in poly-N-isopropylacrylamide-based polymeric nanoparticles. *Int. J. Nanomed.* **2018**, *Volume 13*, 235.
(54) Arakha, M.; Pal, S.; Samantarrai, D.; Panigrahi, T. K.; Mallick, B. C.; Pramanik, K.; Mallick, B.; Jha, S. Antimicrobial activity of iron oxide nanoparticle upon modulation of nanoparticle-bacteria interface. *Sci. Rep.* **2015**, *5*, 1−12.
(55) Siddiqi, K. S.; Husen, A.; Rao, A. K. A review on biosynthesis of silver nanoparticles and their biocidal properties. *J. Nanobiotechnol.* **2018**, *16*, 1−28.
(56) Wang, L.; Hu, C.; Shao, L. The antimicrobial activity of nanoparticles: present situation and prospects for the future. *Int. J. Nanomed.* **2017**, *12*, 1227.
(57) Hayden, S. C.; Zhao, G.; Saha, K.; Phillips, R. L.; Li, X.; Miranda, O. R.; Rotello, V. M.; El-Sayed, M. A.; Schmidt-Krey, I.; Bunz, U. H. F. Aggregation and interaction of cationic nanoparticles on bacterial surfaces. *J. Am. Chem. Soc.* **2012**, *134*, 6920−6923.
(58) Espinosa-Cristóbal, L. F.; Martínez-Castañón, G. A.; Martínez-Martínez, R. E.; Loyola-Rodríguez, J. P.; Patiño-Marín, N.; Reyes-Macías, J. F.; Ruiz, F. Antibacterial effect of silver nanoparticles against Streptococcus mutans. *Mater. Lett.* **2009**, *63*, 2603−2606.
(59) Kalia, A.; Manchanda, P.; Bhardwaj, S.; Singh, G. Biosynthesized silver nanoparticles from aqueous extracts of sweet lime fruit and callus tissues possess variable antioxidant and antimicrobial potentials. *Inorg. Nano-Met. Chem.* **2020**, *50*, 1053−1062.
(60) de Lacerda Coriolano, D.; de Souza, J. B.; Bueno, E. V.; Medeiros, S. M. d. F. R.; Cavalcanti, I. D. L.; Cavalcanti, I. M. F. Antibacterial and antibiofilm potential of silver nanoparticles against antibiotic-sensitive and multidrug-resistant Pseudomonas aeruginosa strains. *Braz. J. Microbiol.* **2021**, *52*, 267−278.
(61) Dong, Y.; Zhu, H.; Shen, Y.; Zhang, W.; Zhang, L. Antibacterial activity of silver nanoparticles of different particle size against Vibrio Natriegens. *PLoS One* **2019**, *14*, No. e0222322.
(62) Adams, L. K.; Lyon, D. Y.; Alvarez, P. J. J. Comparative eco-toxicity of nanoscale TiO_2, SiO_2, and ZnO water suspensions. *Water Res.* **2006**, *40*, 3527−3532.
(63) Kim, D. H.; Park, J. C.; Jeon, G. E.; Kim, C. S.; Seo, J. H. Effect of the size and shape of silver nanoparticles on bacterial growth and metabolism by monitoring optical density and fluorescence intensity. *Biotechnol. Bioprocess Eng.* **2017**, *22*, 210−217.
(64) Oves, M.; Rauf, M. A.; Hussain, A.; Qari, H. A.; Khan, A. A. P.; Muhammad, P.; Rehman, M. T.; Alajmi, M. F.; Ismail, I. I. M. Antibacterial silver nanomaterial synthesis from Mesoflavibacter zeaxanthinifaciens and targeting biofilm formation. *Front. Pharmacol.* **2019**, *10*, 801.
(65) Mapara, N.; Sharma, M.; Shriram, V.; Bharadwaj, R.; Mohite, K.; Kumar, V. Antimicrobial potentials of Helicteres isora silver nanoparticles against extensively drug-resistant (XDR) clinical isolates of Pseudomonas aeruginosa. *Appl. Microbiol. Biotechnol.* **2015**, *99*, 10655−10667.
(66) Nasar, M. Q.; Khalil, A. T.; Ali, M.; Shah, M.; Ayaz, M.; Shinwari, Z. K. Phytochemical Analysis, Ephedra Procera C. A. Mey. Mediated Green Synthesis of Silver Nanoparticles, Their Cytotoxic and Antimicrobial Potentials. *Medicina* **2019**, *55*, 369.
(67) Kim, E.; Maeng, J.-H.; Lee, D. H.; Kim, J. M. Correlation of biomarkers and histological responses in manufactured silver nanoparticle toxicity. *J. Toxicol. Environ. Health Sci.* **2009**, *1*, 8−16.
(68) Tiwari, D. K.; Jin, T.; Behari, J. Dose-dependent in-vivo toxicity assessment of silver nanoparticle in Wistar rats. *Toxicol. Mech. Methods* **2011**, *21*, 13−24.
(69) Guo, H.; Zhang, J.; Boudreau, M.; Meng, J.; Yin, J.-j.; Liu, J.; Xu, H. Intravenous administration of silver nanoparticles causes organ toxicity through intracellular ROS-related loss of inter-endothelial junction. *Part. Fibre Toxicol.* **2015**, *13*, 1−13.
(70) Lee, Y.; Kim, P.; Yoon, J.; Lee, B.; Choi, K.; Kil, K.-H.; Park, K. Serum kinetics, distribution and excretion of silver in rabbits following 28 days after a single intravenous injection of silver nanoparticles. *Nanotoxicology* **2012**, *7*, 1120−1130.
(71) Park, K.; Park, E.-J.; Chun, I. K.; Choi, K.; Lee, S. H.; Yoon, J.; Lee, B. C. Bioavailability and toxicokinetics of citrate-coated silver nanoparticles in rats. *Arch. Pharm. Res. (Seoul)* **2011**, *34*, 153−158.
(72) Recordati, C.; De Maglie, M.; Bianchessi, S.; Argentiere, S.; Cella, C.; Mattiello, S.; Cubadda, F.; Aureli, F.; D'Amato, M.; Raggi, A. J. P.; Lenardi, f.; Milani, P.; Scanziani, E. Tissue distribution and acute toxicity of silver after single intravenous administration in mice: nano-specific and size-dependent effects. *Part. Fibre Toxicol.* **2015**, *13*, 1−17.
(73) Lankveld, D. P.; Oomen, A. G.; Krystek, P.; Neigh, A.; Troost −de Jong, A.; Noorlander, C.; Van Eijkeren, J.; Geertsma, R.; De Jong, W. J. B. The kinetics of the tissue distribution of silver nanoparticles of different sizes. *Biomaterials* **2010**, *31*, 8350−8361.
(74) Ashajyothi, C.; Kelmani Chandrakanth, R. A pilot toxicology study of biogenic silver nanoparticles: in vivo by intraperitoneal and intravenous infusion routes in rats. *J. Exp. Nanosci.* **2019**, *14*, 89−106.
(75) Wang, Z.; Qu, G.; Su, L.; Wang, L.; Yang, Z.; Jiang, J.; Liu, S.; Jiang, G. Evaluation of the biological fate and the transport through biological barriers of nanosilver in mice. *Curr. Pharm. Des.* **2013**, *19*, 6691−6697.
(76) Samberg, M. E.; Oldenburg, S. J.; Monteiro-Riviere, N. A. Evaluation of silver nanoparticle toxicity in skin in vivo and keratinocytes in vitro. *Environ. Health Perspect.* **2010**, *118*, 407−413.

https://doi.org/10.1021/acsomega.2c01922
ACS Omega 2022, 7, 27216−27229